Interfacial thermal transport between nanotubes

S. Kumar[1,a)] and J. Y. Murthy[2]
[1]*Woodruff School of Mechanical Engineering, Georgia Institute of Technology, Atlanta, Georgia 30332, USA*
[2]*School of Mechanical Engineering, Purdue University, West Lafayette, Indiana 47907, USA*

(Received 1 April 2009; accepted 20 September 2009; published online 19 October 2009)

There has been a significant amount of research in analyzing the thermal, electrical, and other physical properties of carbon nanotubes (CNTs). However, the energy transport mechanism at the contact of two CNTs is still not well understood. This study investigates the interfacial thermal interaction between two CNTs using molecular dynamics simulation and wavelet methods. We place the tubes in a crossed configuration and pass a high temperature pulse along one of the CNTs, while keeping other ends fixed, and analyze the interaction of this pulse with the other nanotube. We apply this technique to nanotubes of chirality ranging from (5,0) to (10,0) to observe the response of tubes with changing diameter. This thermal pulse analysis shows that the coupling between the two tubes is very weak and may be dominated by slow-moving phonon modes with high energy. We perform a wavelet analysis of thermal pulse propagation along a CNT and its impact on another CNT in cross contact. Wavelet transformations of the heat pulse show how different phonon modes are excited and how they evolve and propagate along the tube axis depending on its chirality. © *2009 American Institute of Physics*. [doi:10.1063/1.3245388]

I. INTRODUCTION

In recent years, carbon-based nanomaterials, nanotubes, and graphene have attracted a lot of attention because of their unique electrical, thermal, and mechanical properties and their potential application to a wide range of products.[1–5] Carbon nanotubes (CNTs) have been intensively investigated in diverse applications including sensors,[1] electronic displays, energy conversion devices, energy storage,[6–8] and various other electronic and thermal management applications.[3,9] The thermal conductivity of an individual CNT has been measured to be as high as 3400 W/m K,[10] but once embedded inside a composite, the thermal resistance between CNTs and between CNTs and the surrounding material may become the bottleneck for heat transport in these applications. It is very important to understand the transport mechanisms at the interface between CNTs and between CNTs and the substrate to engineer thermal properties and to promote effective removal of heat from CNT-based devices.

It has been observed that percolation behavior for thermal transport in CNT-based composites is suppressed even for CNT densities much higher than the percolation threshold of the nanotube network.[11] However, a corresponding increase in the electrical conductivity has been observed at this threshold, which is an indication of the absence of the thermal percolation effects. It has been suggested before that high tube-to-tube resistance and high tube-to-substrate resistance are responsible for this behavior.[11] However, the thermal transport mechanism at the CNT-CNT contacts in percolation networks has not been well explored. It has also been conjectured that phonons affect electron tunneling transport in CNTs.[10] A firm understanding of CNT-CNT and CNT-substrate interfacial transport may provide guidelines for improving the efficiency and reliability of CNT-based devices.

Various experimental and numerical studies have been performed to estimate the thermal conductivity of CNTs and also to measure the thermal resistance between the CNT and substrate. Most numerical studies are based on the molecular dynamics (MD) method.[10,12] A list of these studies may be found in Ref. 10. Small *et al.* measured the tube-to-substrate resistance (on a per-length basis) of 12 K m/W for a multiwalled CNT sitting on a substrate[13] and Maune *et al.* determined the thermal resistance between a single-walled CNT (SWCNT) and a solid sapphire substrate as 3 K m/W.[14] Recently, Carlborg *et al.* studied the thermal boundary resistance and heat transfer mechanism between CNTs and an argon matrix using MD.[15]

Recent MD computations[12,16] have found high values for tube-tube contact resistance. Maruyama *et al.* used MD simulations to compute the thermal boundary resistance between CNTs surrounded by six other CNTs using the lumped capacitance method.[12] By measuring the transient temperature change in CNTs, they computed the CNT-CNT thermal resistance and found it to be of the order of 1.0×10^{-7} m^2 K/W.[12] Zhong and Lukes considered heat transfer between CNTs using classical MD simulations and estimated the interfacial thermal transport between offset parallel SWCNT as a function of the CNT spacing, overlap, and length.[16] Greaney and Grossman used MD techniques to understand the effect of resonance on the mechanical energy transfer between CNTs.[17] Recently, it has been shown that the thermal resistance at a CNT-CNT contact should be of the order of 0.3×10^{-12} K/W to match the very low conductivity measured for CNT beds. This has also been verified by atomistic Green's function simulations.[18] Nevertheless, the mechanism of energy transport at the interface of two CNTs is still not well understood and needs a detailed exploration.

a)Electronic mail: satish.kumar@me.gatech.edu.

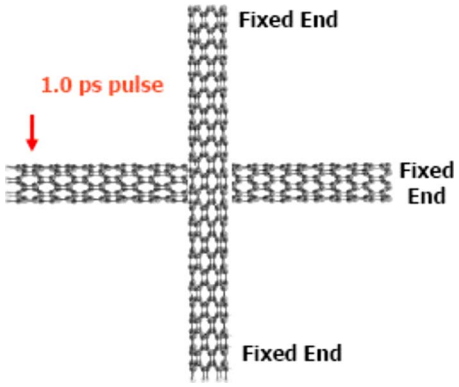

FIG. 1. (Color online) Schematic of two CNTs in a crossed configuration. A 1.0 ps pulse is generated from one end of the first tube, while atoms at the other end are kept fixed. The two ends of the other tube are kept fixed. The chiralities of the two tubes are the same.

Experimental techniques for direct measurement of CNT-CNT resistance have not yet been reported; thus atomistic-level simulations are a vital tool with which to analyze the interfacial transport mechanism.

Our ultimate interest is in identifying the dominant phonon modes for CNT-CNT interaction and in exploring their relation to interfacial thermal resistance. In the present study, we analyze the thermal transport physics between two CNTs using MD simulations and wavelet methods. The CNTs are in contact, but are not bonded. We investigate the thermal interaction between two CNTs in a crossed configuration when a high temperature pulse is passed along one of the CNTs. The application of a strong heat pulse generates several waves propagating at different speeds corresponding to different phonon modes. Using the heat pulse generation methodology previously used by Osman and Srivastava,[19] we investigate how the pulse in one CNT interacts with the other CNT. We analyze how changing the chirality of the CNT affects the interaction between tubes. We then perform a wavelet analysis of thermal pulse propagation along a CNT and its impact on another CNT in cross contact. Wavelet analysis decomposes the time series of the heat pulse in the time-frequency space and helps determine the dominant modes.

II. MD SIMULATION APPROACH

We study the physics of thermal energy transport from one SWCNT to another SWCNT positioned in a crossed configuration and subjected to an intense heat pulse using MD techniques. A schematic of two CNTs in a crossed configuration is shown in Fig. 1. Here, the CNTs are placed perpendicular to each other with a gap equal to a van der Waals distance of 3.4 Å. Selection of appropriate interatomic energies and forces is important for the reliability of classical MD simulations. We use the reactive empirical bond order (REBO) potential for C–C bond interaction and a truncated 12-6 type Lennard-Jones (LJ) potential for nonbonded van der Waals interactions between CNTs. The REBO potential has been extensively applied to perform MD simulations in CNTs and CNTs in hydrocarbon composites/suspensions.[10] The analytical form of this potential is based on the intramolecular potential energy originally derived by Abell Brenner *et al.*[20] The REBO potential is given by

$$U_{\mathrm{REBO}} = \sum_{i} \sum_{i<j} [V_r(r_{ij}) - D_{ij} V_a(r_{ij})], \tag{1}$$

where r_{ij} denotes the distance between atoms i and j, V_r corresponds to interatomic core-core repulsive interactions, and V_a describes the attractive interactions due to the valence electrons. Here, D_{ij} corresponds to a many-body empirical bond order term. The 12-6 type LJ potential for non bonded van der Waals interaction between individual carbon atoms is given as[16]

$$U_{\mathrm{LJ}} = 4\varepsilon \left[\left(\frac{\sigma}{r} \right)^{12} - \left(\frac{\sigma}{r} \right)^{6} \right]. \tag{2}$$

Several different values of the energy and distance parameters in the LJ potential are considered for the interaction of C–C atoms in the CNT. The present study employs the parametrization used by Zhang and Lukes, with $\varepsilon = 4.41$ meV and $\sigma = 0.228$ nm. The details of the MD code used for the present analysis may be found in Ref. 20.

MD simulations are used to examine transient heat pulse propagation in zigzag tubes positioned in a crossed configuration for chiralities varying from (5,0) to (10,0). We generate the heat pulse at one end of the tube using the methodology proposed by Osman and Srivastava[19] for studying energy transport through a single CNT at low temperatures. In order to study heat pulse propagation in CNTs and to compare the results for different chiralities, each CNT is divided into 500 slabs along its axis (each slab is a ring). The length of each CNT is 106 nm, but the number of atoms in a slab depends on the chirality or diameter of the CNT, i.e., a single slab in the (5,0), (6,0), (7,0), (8,0), and (10,0) CNT would have 10, 12, 14, 16, and 20 atoms, respectively. One end of the first CNT, where the heat pulse is generated, is treated as a free boundary, while the other end is kept rigid (see Fig. 1); both ends of the second CNT are held rigid. The boundary region of the first CNT (i.e., the CNT in which the pulse is generated) extends over ten slabs. Before the generation of the heat pulse, both CNTs are quenched to a very low temperature of 0.01 K for 50 000 time steps (25 ps) to achieve thermal equilibrium at 0.01 K. Then, a strong heat pulse of 1 ps duration and a peak temperature of 800 K is generated at one end of the first CNT. The heat pulse is applied to ten slabs near the left boundary using a Berendsen thermostat.[21] The heat pulse consists of a 0.05 ps rise time, a 0.9 ps duration with a constant temperature of 800 K, and a 0.05 ps fall time. During the 0.05 ps fall time, the temperature of the boundary slabs is decreased to reach a final temperature of 0.01 K and then held constant at that temperature for the rest of the simulation. This is done to prevent the exchange of large amounts of energy from the boundary slabs to the region of interest after the generated pulse has started propagating toward the right boundary of the first CNT.

Our analysis is focused on the time window from the point of generation of the pulse to the time before heat pulse reaches the right boundary to avoid the effects of boundary

reflection. The temperature of each slab is spatially averaged over ten slabs centered at the slab of interest. In our simulations, the temperature is time averaged over sets of 200 time steps ($\sim$100 fs) to reduce the effect of statistical fluctuations and is recorded during the entire simulation time. The speed of the pulse is determined from the spatial distance traversed by the particular pulse during a given time interval.

In the above formulation, T, the average temperature of all atoms of a ring at the location of the ring, is defined using equipartition so that

$$3nk_BT = \sum_{i}^{n} m_i v_i^2. \tag{3}$$

Here each ring has n atoms with masses m_i and velocities v_i, and k_B is Boltzmann's constant.

III. WAVELET METHOD

Wavelet analysis of the heat pulse excited in the second CNT is performed for different chiralities of the tubes. The wavelet transform (WT) is an analysis tool well suited for the study of processes which occur over finite spatial and temporal domains. The WT is a generalized form of the Fourier transform. A WT uses generalized local functions known as wavelets which can be stretched and translated with a desired resolution in both the frequency and time domains.[22,23]

Wavelets decompose a time series in the time-frequency space and are useful for identifying the evolution of dominant frequency modes with time. A time signal $s(t)$ is decomposed using wavelet methods in terms of the elementary function $\psi_{b,a}$ derived from a mother wavelet ψ by dilation and translation,[22]

$$\psi_{b,a}(t) = \frac{1}{a^{0.5}}\psi\left(\frac{t-b}{a}\right). \tag{4}$$

Here, a and b are parameters that control dilation and translation, respectively. The a parameter is also known as the *scale* in wavelet analysis. $\psi_{b,a}$ is known as the *daughter* wavelet as it is derived from the mother wavelet ψ using translation and dilation. The normalization factor $a^{0.5}$ ensures that the mother and daughter wavelets have the same energy. The WT of a signal $s(t)$ is given as the convolution integral of $s(t)$ with ψ^*, where ψ^* is the complex conjugate of the wavelet function ψ,

$$W(b,a) = \frac{1}{a^{0.5}}\int \psi^*\left(\frac{t-b}{a}\right)s(t)dt. \tag{5}$$

In general, wavelet functions are complex functions, so the WT are also complex and have a real part, an imaginary part, and a phase angle. The power spectrum of a WT is defined as $|W|^2$. We use the Morlet wavelet for heat pulse analysis; this wavelet has the form of a plane wave with a Gaussian envelope.[22] The Morlet wavelet is given by

$$\psi = e^{iwt} \times e^{-0.5|t|^2}. \tag{6}$$

The form of this wavelet is shown in Fig. 2 after translating by different values of b and dilating by different values of the scale parameter a.

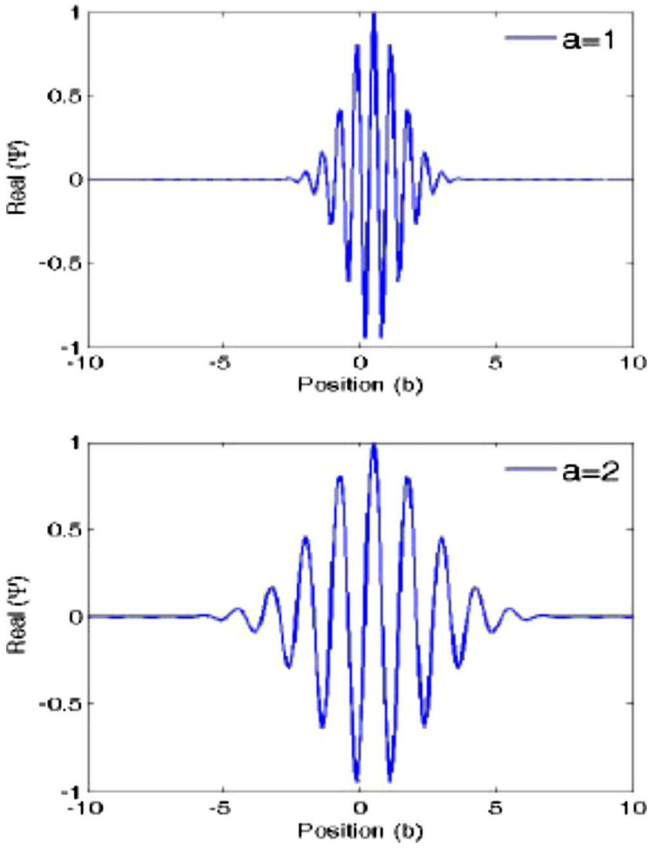

FIG. 2. (Color online) An example of a Morlet wavelet (Ref. 22) with different values of scale a.

The power spectrum of the velocity magnitude of each atom in the nanotube is computed using the method described above. By summing the power spectrum over all the atoms of one ring, a one-dimensional projection of the temporal spectra along the nanotube axis is obtained. In this way, temporally evolving spectra of the velocity magnitude for the entire spatiotemporal field are obtained.

IV. HEAT PULSE ANALYSIS

We first study the interaction between two CNTs in a crossed configuration when a heat pulse is passed through first CNT using the methodology described in the above sections. Our interest is in analyzing the energy transfer to the second tube when the heat pulse passes through the contact zone and also to study the waves generated in the second tube due to this energy transfer. The distance between the CNTs remains in the range of 3–3.7 Å during the entire simulation for CNTs of (5,0), (6,0), and (7,0) chiralities. For CNTs of (8,0) chirality, this distance remains in the range of 4–4.5 Å, while for CNTs of (10,0) chirality, it remains in the range of 5–5.5 Å.

The location and shape of the heat pulses at different time instants along the first and second CNTs for the case of (5,0) chirality are shown in Figs. 3(a) and 3(b), respectively. The amplitude of the heat pulses is presented in terms of the average kinetic energy of the atoms in ten slabs at any location. Here, $t=0$ ps corresponds to the time when heat pulse generation has started at the left end of the first CNT. The

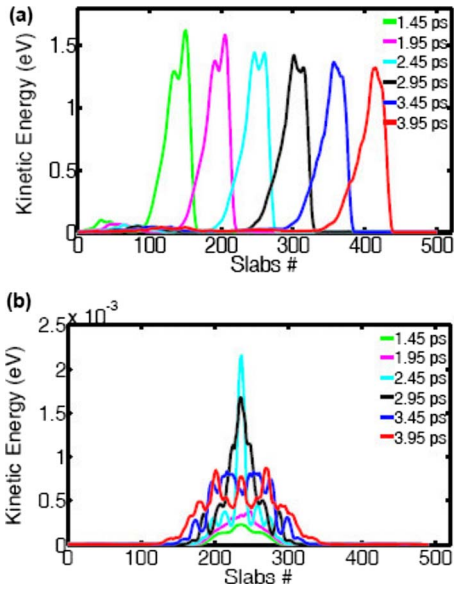

FIG. 3. (Color online) (a) The location and shape of the heat pulse at different time instants along the first CNT for (5,0) chirality. The pulse generation started at $t=0.0$ ps. (b) The location and shape of the heat pulse at different time instants in the second CNT, also of the same chirality.

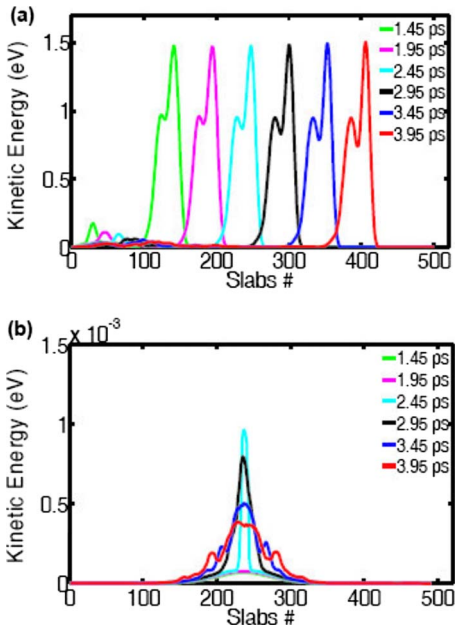

FIG. 4. (Color online) (a) The location and shape of the heat pulse at different time instants along the first CNT for (7,0) chirality. The pulse generation started at $t=0.0$ ps. (b) The location and shape of the heat pulse at different time instants in the second CNT, also of the same chirality.

attenuation in peak kinetic energy (~ 1.2 eV) of the heat pulse is negligible and it is seen to propagate like a ballistic pulse along the first tube. This pulse moves with a speed of 22 km/s along the nanotube, which is very close to the speed of sound (20.3 km/s) associated with longitudinal acoustic (LA) phonon waves in zigzag nanotubes.[19] Two CNTs located in a crossed configuration make contact at their midpoint, which is at 53 nm from their free ends. When the heat pulse in the first tube approaches this contact zone, the kinetic energy in the other tube increases at the location of the contact [Fig. 3(b)]. The kinetic energy reaches its maximum at $t=2.6$ ps, which is approximately the time taken by the heat pulse in the first tube to cross the contact zone. The peak kinetic energy in the second tube is 1.5 meV, which is very low in comparison to peak kinetic energy of 1.2 eV of the heat pulse in the first tube. This indicates that coupling is very weak between two CNTs for these fast moving pulses since little time is spent by the pulse in the contact zone. The energy given to the second tube at the point of contact spreads along the second tube. This is indicated by the decreasing kinetic energy at the center of the second tube and the symmetrically excited heat pulses on both sides of the contact in Fig. 3(b). The speed of propagation of the excited heat pulse in the second tube is very low and it is difficult to relate these pulses with any specific phonon mode by observing their transient propagation profiles.

We perform a similar heat pulse analysis for nanotubes of (6,0), (7,0), (8,0), and (10,0) chiralities; the shape and location of the heat pulse along the nanotube for different time instants for the (7,0), (8,0), and (10,0) chiralities are shown in Figs. 4–6. It is observed that the behavior of heat pulses in the nanotubes is very dependent on the chirality or the diameter of the tube. The speed of heat pulse propagation in the first tube and the increase in kinetic energy in the second tube until $t=5.5$ ps are listed in Table I. Heat pulse propagation in the first tube for (6,0) and (7,0) chiralities is similar to that for the (5,0) nanotube, i.e., the heat pulse propagates like a ballistic wave with a speed in the range of 22–23 km/s. However, the pulses excited in the second tube are significantly different for different chirality tubes. No conclusions can be drawn merely by looking at the kinetic energy rise in the second tube (see Table I). However, it can be observed that heat spreading along the second tube is faster in the (5,0) tube in comparison to the (6,0) and (7,0)

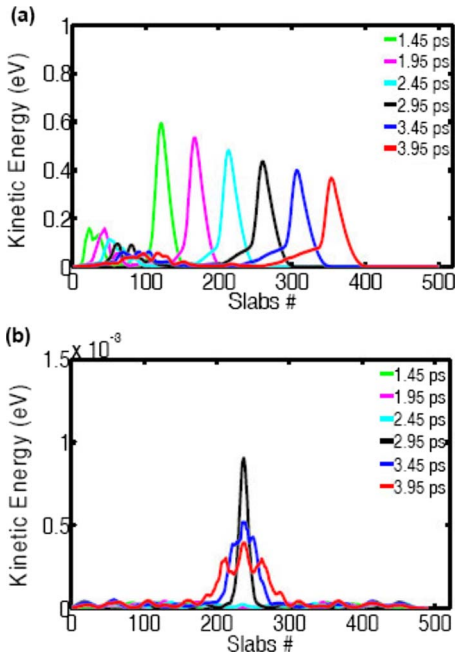

FIG. 5. (Color online) (a) The location and shape of the heat pulse at different time instants along the first CNT for (8,0) chirality. The pulse generation started at $t=0.0$ ps. (b) The location and shape of the heat pulse at different time instants in the second CNT, also of the same chirality.

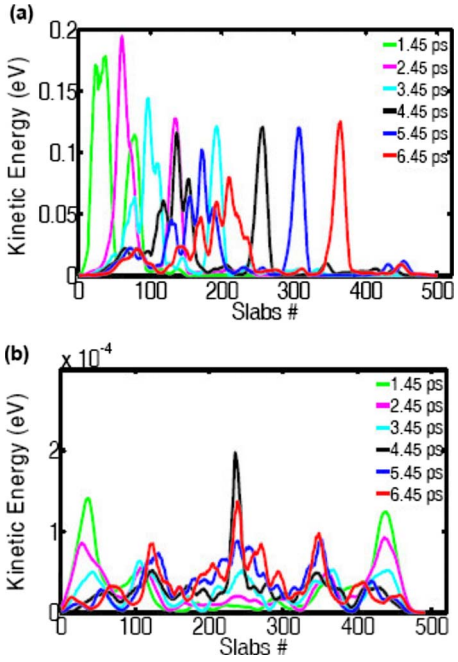

FIG. 6. (Color online) (a) The location and shape of the heat pulse at different time instants along the first CNT for (10,0) chirality. The pulse generation started at $t=0.0$ ps. (b) The location and shape of the heat pulse at different time instants in the second CNT, also of the same chirality.

tubes (see Figs. 3 and 4). It is also observed that the kinetic energy at the center of the second tube drops relatively fast in the (6,0) tube in comparison to the (7,0) tube.

Heat pulse propagation is completely different for (8,0) and higher chirality tubes. For the (8,0) tube, the heat pulse decays while propagating along the first tube and also broadens with time, a behavior which is completely different from that observed in low-chirality tubes. At time $t=1.45$ ps, the peak kinetic energy of the pulse is 0.68 eV and decays to 0.42 eV at $t=3.95$ ps [Fig. 5(a)]. The pulse speed in the (8,0) tube is 19 km/s, which is lower than the pulse speed observed in lower-chirality tubes (see Table I). Oman and Srivastava[19] observed a similar decay in the pulse speed in zigzag tubes for twisting phonon modes with speed in the range of 16–18 km/s. The pulse excited in the second tube also shows different characteristics and exhibits a pulse shape that is more flat at the center [Fig. 5(b)]. All these behaviors imply a dissipative nature to the pulse propagation in the (8,0) tubes.

Heat pulse propagation in a (10,0) tube is much different from that previously discussed for tubes of low chirality. The high kinetic energy in the heat pulse in the first tube cannot be sustained and the pulse decays very quickly. At $t=2.45$ ps, a clearly identifiable wave shape evolves from the dissipating heat pulse; the speed of this wave is 12.5 km/s, which corresponds to the second sound wave speed observed in zigzag tubes in Ref. 19. In transient experiments, at low temperatures and in structures with high purity, normal phonon scattering processes can play an important role. They may couple various phonon modes and make the collective oscillation in phonon density possible which is a second sound. The second sound is observed under very restrictive conditions.[19] One of these conditions is that the momentum conserving normal phonon scattering processes should be dominant compared to the momentum randomizing Umklapp phonon scattering processes.[19] For CNTs, the thermal conductivity increases even up to room temperature and it can reasonably be believed that *N*-process phonon interactions dominate over a wide range of temperature. These arguments and the observed speed of the wave (12.5 km/s$=1/3^{0.5}$ times the LA phonon speed) suggest that the observed wave pulse in the (10,0) nanotube corresponds to that of the second sound.

TABLE I. Pulse speed in the first tube and the maximum total energy rise in the second tube for different chiralities.

CNT chirality	Pulse speed (km/s)	Increase in the total energy of the second tube until $t=5.5$ ps (eV)
(5,0)	22.0	0.129
(6,0)	23.2	0.203
(7,0)	22.6	0.046
(8,0)	19.0	0.074
(10,0)	12.5	0.037

The peak kinetic energy of the second sound wave mode observed in the (10,0) tube is 0.12 eV, which is much smaller than the peak kinetic energy of the leading heat pulses observed in the low-chiral tube configurations. In addition, due to the low speed, this pulse in the first CNT does not cross the contact zone in 4 ps (this is the time range for which we analyzed low-chirality tubes), so we have extended the analysis up to 6.5 ps. The energy gained by the second CNT due to the interaction with the heat pulse of the first CNT is very low. This is the reason for a very small rise in the peak kinetic energy ($\sim$0.2 meV) of the excited pulse in the second tube [Fig. 6(b)]. The kinetic energy of the carbon atoms located at the contact area of the second CNT [black and red curves in Fig. 6(b)] is of the same order as that of the kinetic energy of atoms at other locations [see peaks at the CNT ends in Fig. 6(b)].

From our analysis, we have observed that in low-chirality CNTs, we can generate a purely ballistic pulse, while in high-chirality CNTs, a diffusive tail is also present and the pulse cannot sustain its peak temperature during propagation. We see a difference between our results and Osman and Srivastava's results only for low-chirality CNTs. The observed differences may be due to the boundary conditions at the CNT ends or the method used to prepare the system before the pulse is generated. Osman and Srivastava's calculation uses a reflective boundary condition at the ends of the CNT where the heat pulse is applied, while we have considered free ends without a reflective boundary condition. In addition, the system preparation method may be another reason for the possible difference.

The change in the total energy of the CNTs as a function of time is plotted in Fig. 7 for the (6,0), (7,0), (8,0) and (10,0) tubes. The change in the total energy is computed with respect to the reference total energy at $t=1$ ps; this is the time at which the pulse generated in the first CNT starts propagating toward the contact region of the two CNTs. The

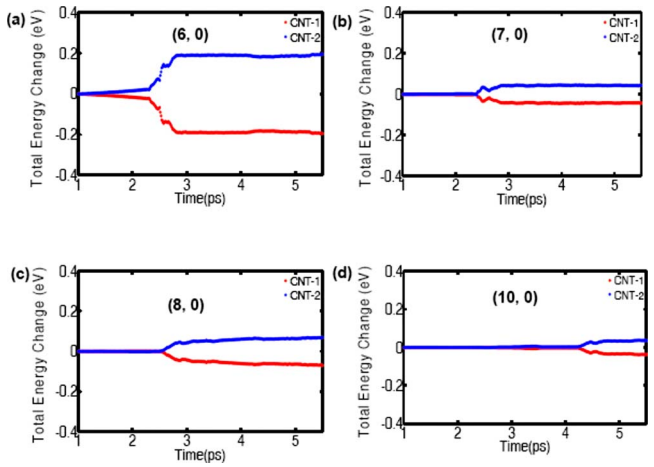

FIG. 7. (Color online) Change in the total energy of CNTs as a function of time with reference total energy corresponding to $t=1$ ps. At $t=1$ ps, the pulse generated in CNT-1 starts to propagate toward the contact region of the two CNTs. Here, CNT-1 corresponds to the CNT in which the pulse is generated; CNT-2 is located in a crossed configuration with respect to CNT-1. The chiralities of the CNTs are (a) (6,0) (b) (7,0) (c) (8,0), and (d) (10,0).

magnitude of the total energy exchange or increase in the total energy of the second tube up to time instant 5.5 ps is presented in Table I for tubes of different chiralities. The energy exchange between the tubes is the largest for the (6,0) tube and decreases for high-chirality tubes (Fig. 7). However, a definitive statement regarding this cannot be made based on the present analysis as the energy exchange for the (5,0) tube is lower than that for the (6,0) tube by 0.07 eV and the energy exchange for the (7,0) tube is lower than that for the (8,0) tube by 0.028 eV. The above analysis shows that lower-chirality tubes have better coupling in comparison to high-chirality tubes as far as these heat pulses are concerned. Phonon modes with high speed are very inefficient in transferring energy to the second tube as they spend very little time in the contact zone. Thus, it is likely that for realistic applications, slow-moving phonon modes (for example, optical modes) in the first CNT would be better coupled to the second CNT. Shiomi and Maruyama[24] observed from their modal analyses on a single tube using wavelet transformations that the major contribution to non-Fourier heat conduction comes from optical phonon modes with sufficient group velocity and with wave vectors in the intermediate regime for short nanotubes. Dispersion curves for CNTs of (5,5) chirality show that even at low frequencies, longitudinal and transverse optical modes may be present, with velocities comparable to the acoustic modes. In a nanotube network, the link between two nanotubes is of the order of just few nanometers. Therefore, in nanotube networks where the contact between the tubes governs the transport, optical phonon modes may be a dominant heat transfer pathway for communication between tubes.

V. WAVELET ANALYSIS

Wavelet analysis of the energy modes excited in the second CNT due to the interaction with the first CNT is performed for chirality of tubes varying from (5,0) to (10,0).

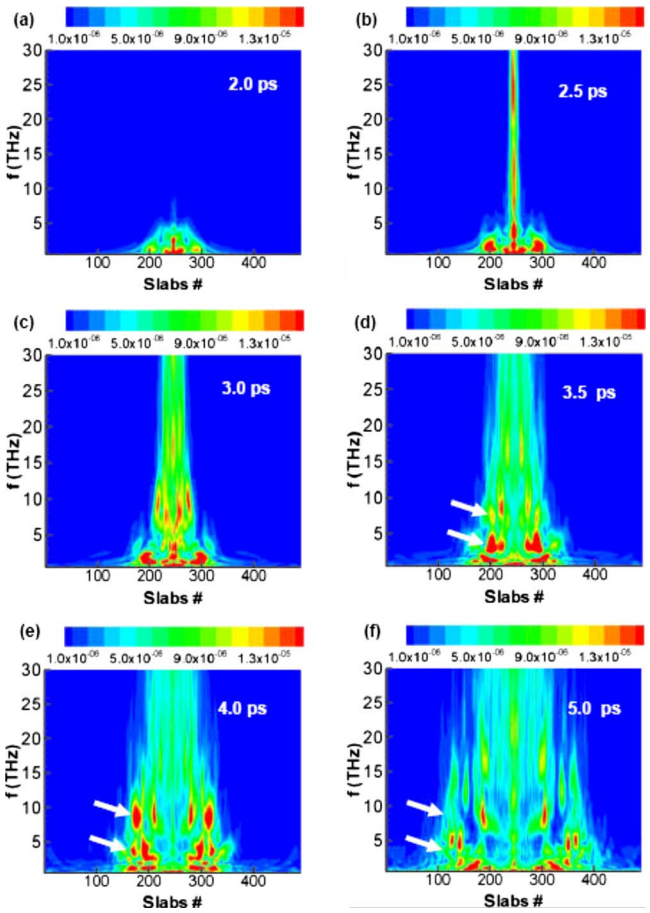

FIG. 8. (Color online) Frequency spectrum along the second nanotube for (5,0) chirality at different time instants: (a) 2.0 ps, (b) 2.5 ps, (c) 3.0 ps, (d) 3.5 ps, (e) 4.0 ps, and (f) 5.0 ps. White arrows show frequencies corresponding to 5 and 10 THz.

The power spectrum of the velocity magnitude of each atom in the nanotube is computed using the method described in Sec. III. Temporally evolving spectra of the velocity magnitude for the entire spatiotemporal field are computed. The results are presented as temporal sequences of the spectral contours in the frequency space domain in Fig. 8 for a (5,0) CNT. Six temporal sequences are used, which correspond to $t=2.0$, 2.5, 3.0, 3.5, 4.0, and 5.0 ps. In these plots, the vertical axis represents the frequency in terahertz and the horizontal axis represents the spatial location along the nanotube axis in terms of the slab (i.e., ring) numbers.

The evolution and propagation of spectral modes along the tube axis for a (5,0) CNT at different time instants may be observed in Fig. 8. At $t=2$ ps, the heat pulse in the first tube is approaching the contact zone [Fig. 8(a)]; thus, some low frequency phonon modes are excited in the second nanotube at the location of the contact. At $t=2.5$ ps [Fig. 8(b)], the heat pulse in the first tube crosses the contact zone; this is the time at which the peak temperature of the thermal pulse excited in the second CNT is observed [see Fig. 3(b)]. Phonon modes of frequencies up to 30–35 THz are excited in the second nanotube by this time, but most of the dominant frequencies are less than 10 THz [Fig. 8(b)]. Once the heat pulse in the first tube moves away from the contact zone, the energy given to the second tube spreads to both sides of the

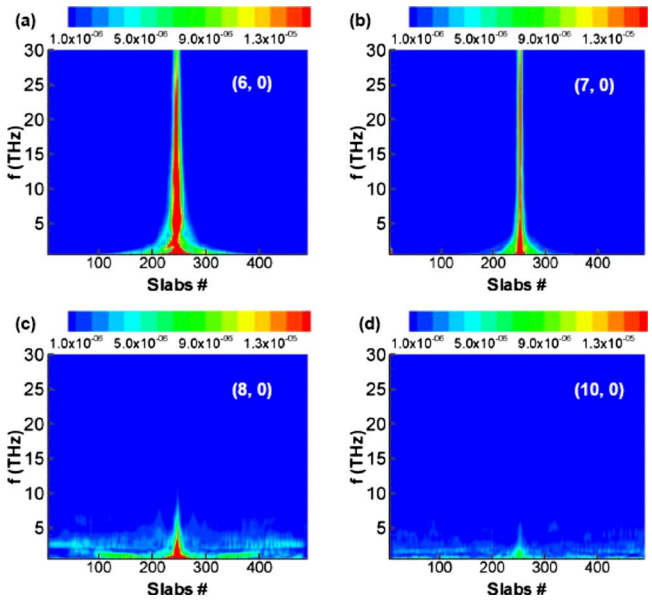

FIG. 9. (Color online) Frequency spectrum along the second CNT at 2.5 ps for chiralities: (a) (6,0), (b) (7,0), (c) (8,0), and (d) (10,0).

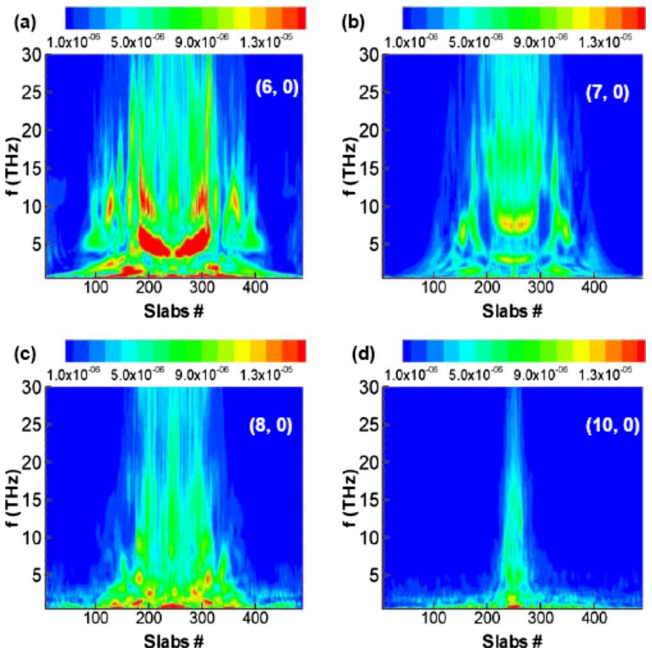

FIG. 10. (Color online) Frequency spectrum along the second CNT at 5.0 ps for chiralities: (a) (6,0), (b) (7,0), (c) (8,0), and (d) (10,0).

tube symmetrically. Different phonon modes are excited along the second tube and can be observed from the contour plots in Figs. 8(c)–8(f). The contour plot at $t=3.0$ ps shows two distinctly visible modes; one centered at around 5 THz and another centered at around 10 THz. The speed of these modes may be computed from the movement of the high power spectrum color patches corresponding to these frequencies along the nanotube axis in the contour plot. The computed speed is 12.0 km/s, which is close to the speed of the second sound waves observed in these zigzag tubes.[19] These color patches are shown in Figs. 8(d)–8(f) by white arrows. Most of the other dominant modes correspond to frequencies even lower than 5 THz, which is in correspondence with the small amount of heat transferred to the second tube from the heat pulse in the first tube.

Contours of the power spectrum for the (6,0), (7,0), (8,0), and (10,0) CNTs at $t=2.5$ and 5.0 ps are shown in Figs. 9 and 10, respectively. As in the case of the (5,0) CNT, two dominant phonon modes corresponding to 5 and 10 THz are seen to propagate along the second tube for the (6,0) and (7,0) CNTs [Figs. 10(a) and 10(b)]. These contour plots also clearly show that the rate of heat spreading along the CNT axis slows down with increasing diameter. This is also observed in the heat pulse analysis in Sec. IV by examining the location and shape of the heat pulses generated in the second tube. A similar comparison cannot be made for the (8,0) and (10,0) CNTs because the pulse generated in the first CNT is not sustained at its initial peak temperature and very little heat is transferred to the second CNT for these cases. The spectral modes for the (10,0) CNT are completely different from other CNTs; most of the high energy modes present in low-chirality CNTs are not excited [Fig. 10(d)]. This is due to the evolution of the second sound waves in the first CNT; the peak temperature is an order of magnitude lower than that in low-chirality CNTs [Fig. 6(b) and 10(d)].

VI. CONCLUSIONS

We analyzed the thermal transport between two CNTs for different chiralities using the MD technique. We arranged two CNTs in a crossed configuration. They were initialized at a very low temperature (0.01 K). A thermal pulse was generated at one end of the first CNT to study the response of the second tube when this pulse passed the contact region of the two CNTs. The behavior of the peak temperature of the propagating pulse is quite different from that observed by Osman and Srivastava.[19] Our simulations show that the heat pulse propagates along the first CNT with the speed of acoustic phonons, retaining its peak temperature of 800 K for the (5,0), (6,0) and (7,0) CNTs. In contrast, Osman and Srivastava[19] observed a diffusive background of very high temperature and other leading wave packets of very low peak temperature but with the characteristic speed of different phonon modes evolving after the heat pulse generation. We observe propagation behavior similar to Osman and Srivastava[19] only for the (10,0) CNT. The physics behind this difference in behavior with respect to low-chirality CNTs is not clearly understood. The results of our heat pulse studies demonstrate that phonon modes with high speed are very inefficient in transferring energy to the second tube as they spend very little time in the contact zone. Most likely, slow-moving phonon modes in the first CNT would be better coupled to the second CNT and would dominate thermal boundary conductance between these CNTs.

Wavelet analysis shows that phonon modes of frequencies up to 30–35 THz are excited in the second CNT when the heat pulse in the first CNT passes the contact zone, but most of the dominant frequencies are less than 10 THz. Two dominant modes centered at around 5 and 10 THz are observed in the (5,0), (6,0), and (7,0) CNTs, with a propagation speed of 12 km/s which corresponds to the speed of the second sound waves.[19] We also observe that the rate of heat

spreading along the CNT axis slows down with increasing diameter, as seen by comparing (5,0) CNT to (7,0) CNT.

The present analysis employs heat pulse propagation and wavelet analysis to study the interaction between CNTs. To better understand the coupling modes between tubes, a wave packet corresponding to specific phone modes should be passed through a CNT and its interaction with other CNTs studied. Understanding the coupling between CNTs of different chiralities and contact areas could also be of great interest for engineering the properties of CNT-network based composites. Most of the present work is in the low temperature regime. It is also important to investigate transport mechanisms in the high temperature regime using either appropriate numerical modeling or experimental techniques.

ACKNOWLEDGMENTS

Support of S.K. and J.Y.M. under NSF Grant No. EEC-0228390 and the Purdue Research Foundation is gratefully acknowledged.

[1]E. S. Snow, F. K. Perkins, E. J. Houser, S. C. Badescu, and T. L. Reinecke, Science **307**, 1942 (2005).
[2]X. J. Xu, M. M. Thwe, C. Shearwood, and K. Liao, Appl. Phys. Lett. **81**, 2833 (2002).
[3]H. Huang, C. Liu, Y. Wu, and S. Fan, Adv. Mater. (Weinheim, Ger.) **17**, 1652 (2005).
[4]A. A. Balandin, S. Ghosh, W. Z. Bao, I. Calizo, D. Teweldebrhan, F. Miao, and C. N. Lau, Nano Lett. **8**, 902 (2008).
[5]M. B. Bryning, D. E. Milkie, M. F. Islam, L. A. Hough, J. M. Kikkawa, and A. G. Yodh, Adv. Mater. (Weinheim, Ger.) **19**, 661 (2007).
[6]S. Kumar, N. Pimparkar, J. Y. Murthy, and M. A. Alam, Appl. Phys. Lett. **88**, 123505 (2006).
[7]C. R. Kagan and P. Andry, *Thin Film Transistors* (Dekker, New York, 2003).
[8]S. Kumar, J. Y. Murthy, and M. A. Alam, Phys. Rev. Lett. **95**, 066802 (2005).
[9]S. Kumar, J. Y. Murthy, and M. A. Alam, Int. J. Nanomanufacturing (IJNM) **2**, 226 (2008).
[10]J. R. Lukes and H. L. Zhong, ASME Trans. J. Heat Transfer **129**, 705 (2007).
[11]S. Kumar, M. A. Alam, and J. Y. Murthy, Appl. Phys. Lett. **90**, 104105 (2007).
[12]S. Maruyama, Y. Igarashi, and Y. Shibuta, *Molecular Dynamics Simulations of Heat Transfer Issues in Carbon Nanotubes*, The 1st International Symposium on Micro & Nano Technology, 14–17 March, 2004, Honolulu, Hawaii, USA.
[13]J. P. Small, L. Shi, and P. Kim, Solid State Commun. **127**, 181 (2003).
[14]H. Maune, H. Y. Chiu, and M. Bockrath, Appl. Phys. Lett. **89**, 013109 (2006).
[15]C. F. Carlborg, J. Shiomi, and S. Maruyama, Phys. Rev. B **78**, 205406 (2008).
[16]H. L. Zhong and J. R. Lukes, Phys. Rev. B **74**, 125403 (2006).
[17]P. A. Greaney and J. C. Grossman, Phys. Rev. Lett. **98**, 125503 (2007).
[18]R. S. Prasher, X. J. Hu, Y. Chalopin, N. Mingo, K. Lofgreen, S. Volz, F. Cleri, and P. Keblinski, Phys. Rev. Lett. **102**, 105901 (2009).
[19]M. A. Osman and D. Srivastava, Phys. Rev. B **72**, 125413 (2005).
[20]D. W. Brenner, O. A. Shenderova, J. A. Harrison, S. J. Stuart, B. Ni, and S. B. Sinnott, J. Phys.: Condens. Matter **14**, 783 (2002).
[21]P. Erhart and K. Albe, Appl. Surf. Sci. **226**, 12 (2004).
[22]K. M. Lau and H. Weng, Bull. Am. Meteorol. Soc. **76**, 2391 (1995).
[23]C. Torrence and G. P. Compo, Bull. Am. Meteorol. Soc. **79**, 61 (1998).
[24]J. Shiomi and S. Maruyama, Phys. Rev. B **73**, 205420 (2006).